Available online at www.sciencedirect.com
SCIENCE DIRECT®
Journal of Sound and Vibration 270 (2004) 539–557
JOURNAL OF SOUND AND VIBRATION
www.elsevier.com/locate/jsvi

The evaluation of non-reflecting boundary conditions for duct acoustic computation

S.K. Richards[a,*], X. Zhang[a], X.X. Chen[b], P.A. Nelson[b]

[a] *School of Engineering Sciences, University of Southampton, Southampton SO17 1BJ, UK*
[b] *Institute of Sound and Vibration, University of Southampton, Southampton SO17 1BJ, UK*

Accepted 15 September 2003

Abstract

A simple method is used to quantify the performance of non-reflecting boundary conditions for duct acoustic applications. The method uses a two-dimensional wavesplitting technique to decompose the linearized Euler equations into its constitutive modes, allowing the magnitude of reflected waves from outflow boundaries to be accurately determined. Realistic conditions are simulated by conducting the boundary condition analysis using acoustic waves with characteristics often found in duct and turbomachinery problems. For this paper, the method is used to investigate the performance of three different buffer zone implementations and the Perfectly Matched Layer as non-reflecting boundary conditions. The effect of the damping properties of these boundary conditions and the incident acoustic wave characteristics on performance are considered. Results indicate that the buffer zone boundary condition using explicit damping of the solution vector after each timestep produces the best non-reflecting performance. A deterioration in performance was observed for incident waves at high angles relative to the boundary normal for all implementations.

1. Introduction

Computational Aeroacoustics (CAA) is the numerical simulation of noise generation and propagation within aerodynamic flows. A major application of CAA has been towards the prediction of noise generated by aircraft components and the corresponding sound level observed in the far field. Noise generation is governed by the Navier–Stokes equations, however, the solution of the Navier–Stokes equations over large domains to determine farfield noise is not

*Corresponding author.
E-mail address: s.k.richards@soton.ac.uk (S.K. Richards).

0022-460X/$ - see front matter © 2004 Published by Elsevier Ltd.
doi:10.1016/j.jsv.2003.09.042

computationally feasible. This may be overcome by the separation of the noise generation and noise propagation processes, with noise propagation being determined by the linearized Euler equations (LEE) which are computationally less intensive than the Navier–Stokes equations. Even so, very large computational domains are still prohibitive, requiring them to be truncated by the introduction of artificial boundaries. Numerical non-reflecting boundary conditions are required at such boundaries to ensure that out-going disturbances are not reflected. With the development of high order discretization schemes for the accurate prediction of noise propagation, it is often spurious reflections from the artificial boundaries that are the greatest source of numerical error in CAA simulations.

In many cases, these reflections can be reduced by manipulation of the domain boundary, such that the outgoing wave angle relative to the boundary is small, giving more favourable reflection properties. However, in duct acoustic problems, this is not possible as the position and geometry of the domain boundary is governed by the shape of the duct. The performance of five non-reflecting boundary conditions in duct acoustic applications is investigated by using a wavesplitting technique developed by Wilson [1], to accurately measure wave reflection from domain boundaries.

A variety of non-reflecting boundary conditions have been developed that reduce spurious reflections at the edges of truncated computational grids. Three of the main types of non-reflecting boundary conditions are characteristic methods, farfield asymptotic solutions and buffer zone techniques. The application of a characteristic analysis of the Euler equations to formulate non-reflecting boundary conditions has been presented by Thompson [2,3], Poinsot and Lele [4] and Giles [5]. The boundary condition is formulated by conducting a one-dimensional characteristic analysis of the Euler equations. From the analysis the boundary equations can be written in characteristic form. A non-reflecting boundary condition is created by assigning the value of the characteristic that represents waves entering at the boundary. Characteristic non-reflecting boundary conditions have been used for a number of CAA simulations [6,7]. Due to the one-dimensional formulation, they perform best when the out-going wave is normal to the grid boundary.

Farfield asymptotic boundary conditions are based upon the asymptotic solution of the governing equations at the farfield boundary [8,9]. Such boundary conditions have been shown to be accurate for some simulations. However, the difficulty in obtaining asymptotic solutions for complex flows means that their scope is limited.

The buffer zone technique is a group of boundary conditions based upon damping methods. For buffer zone techniques the computational grid is extended to create an extra domain (or zone) in which the solution is damped by an application of low-pass filters, grid stretching or numerical damping [10–13]. Another method is to accelerate the flow to supersonic speeds at the end of the buffer zone, eliminating the need for a non-reflecting boundary condition [14]. Buffer zone boundary conditions are easy to implement, but the inclusion of artificial damping within the buffer zone means that the solution is not physical. The addition of extra grid points in the buffer zones adds to the computational cost. The performance of the buffer technique based upon numerical damping methods will be the main aim of investigation in this paper.

A more involved formulation of the numerical damping technique is the Perfectly Matched Layer (PML) [15]. Again extra damping regions are added around the computational domains in which out-going waves are damped. The formulation of the equations solved in the PML means that, in theory, the outgoing waves will not create any reflection when entering a PML domain, for any frequency or wave angle. The first PML boundary condition for the Euler equations was

proposed by Hu [16] and used a split formulation of the Euler equations. A second application of the PML technique to the Euler equations was given by Arbabanel et al. [17]. For both formulations, exponentially growing solutions at the PML/computation domain boundary were observed under certain flow conditions, requiring the inclusion of numerical filtering and artificial damping in order to maintain stable solutions. Recently, Hu [18,19] presented an unsplit stable PML formulation that does not support exponentially growing solutions.

Of the non-reflecting boundary conditions currently used, buffer zone techniques and the PML have been shown to perform well for many test case problems. The simplicity of buffer zone techniques and their applicability to linear and non-linear Euler equations means they hold potential as a general non-reflecting boundary condition for CAA. The damping methods used in buffer zone boundary conditions also form the basis of the numerical implementation of the PML, so an analysis of the buffer zone method will also gain insight into issues relating to the PML method. To date, however, little work has been done to analyse the performance of the different buffer zone techniques and the PML when applied to realistic problems. In this paper, the performance of three different implementations of the buffer zone technique is quantified based upon numerical damping and the PML and the factors affecting their performance are investigated. The analysis is conducted using the linearized Euler equations and the results compared to the performance of Thompson's characteristic boundary condition [3].

A simple method is used to determine the performance of non-reflecting boundary conditions for typical acoustic waves found in duct and turbomachinery noise propagation problems.

2. Governing equations

2.1. Linearized Euler equations

In the following analysis the Linearized Euler equations in a Cartesian co-ordinate system are considered. The equations are linearized about a steady, uniform mean flow in the x-direction. In non-conservative vector form the equations are given by

$$\frac{\partial \mathbf{U}}{\partial t} + [\mathbf{A}]\frac{\partial \mathbf{U}}{\partial x} + [\mathbf{B}]\frac{\partial \mathbf{U}}{\partial y} = 0, \tag{1}$$

where [**U**] is the vector of primitive solution variables

$$[\mathbf{U}] = \begin{bmatrix} \rho' \\ u' \\ v' \\ p' \end{bmatrix},$$

$$[\mathbf{A}] = \begin{bmatrix} U_0 & 1 & 0 & 0 \\ 0 & U_0 & 0 & 1 \\ 0 & 0 & U_0 & 0 \\ 0 & 1 & 0 & U_0 \end{bmatrix}, \quad [\mathbf{B}] = \begin{bmatrix} 0 & 0 & 1 & 0 \\ 0 & 0 & 0 & 0 \\ 0 & 0 & 0 & 1 \\ 0 & 0 & 1 & 0 \end{bmatrix}.$$

Here, ρ is the density, u, v the velocities, p the pressure and U_0 the mean velocity in the x-direction. An apostrophe denotes a fluctuating variable. In Eq. (1), the density is non-dimensionalized by the mean density, ρ_0, all velocity variables by the speed of sound, c, and pressure by $\rho_0 c^2$.

2.2. Boundary conditions

2.2.1. Buffer zone boundary condition

To create a buffer zone boundary condition based upon numerical damping, an extra zone is adjoined on to the edge of the computational domain where the boundary condition is to be applied, see Fig. 1. Within this extra zone, the amplitude of the out-going wave is damped to a set target value by a damping function, $\sigma(x)$. Damping the out-going waves to a target value means that the amplitude of the waves at the outer edge of the buffer zone is constant. Setting a constant amplitude is the non-reflecting criterion upon which buffer zone boundary conditions based upon numerical damping work. The damping function is set to zero at the interface between the computational domain and the buffer zone to allow out-going waves to smoothly enter the buffer zone. Full damping is applied at the outer edge of the buffer zone to damp the target solution. In between, the damping function is varied smoothly to minimize possible reflections.

The performance is investigated of the three main implementations of the buffer zone boundary condition based upon numerical damping.

Type I: The solution vector is explicitly damped after each timestep [10].

$$\mathbf{U}^{n+1} = \overline{\mathbf{U}^{n+1}} - \sigma(\overline{\mathbf{U}^{n+1}} - \mathbf{U}_{target}), \tag{2}$$

where $\overline{\mathbf{U}^{n+1}}$ is the solution vector computed after each time step. The damping coefficient, σ, varies smoothly according to the function

$$\sigma(x) = \sigma_{\max}\left|1 - \frac{x - L}{L}\right|^{\beta}, \tag{3}$$

where L is the width of the buffer zone, x is the distance from the inner boundary of the buffer zone and $\sigma_{\max}$ and β are set coefficients which determine the shape of the damping function. For

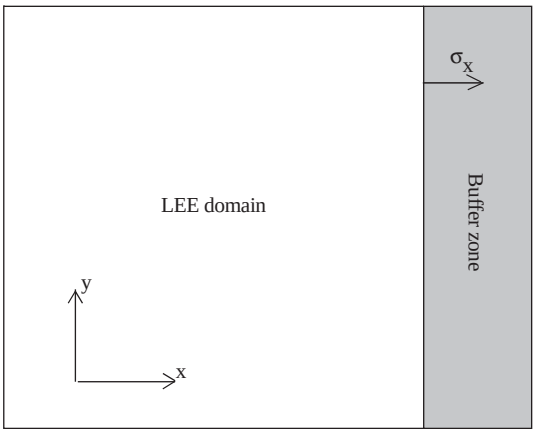

Fig. 1. Schematic of buffer zone implementation.

the LEE the intention is to damp the out-going waves in the buffer zone to the mean flow, hence the target solution $\mathbf{U}_{target}$ is set as zero.

Type II: Implicit damping where the damping term is included in the governing equations [11]. With this added damping term, equations to be solved in the buffer zone become

$$\frac{\partial \mathbf{U}}{\partial t} + [\mathbf{A}]\frac{\partial \mathbf{U}}{\partial x} + [\mathbf{B}]\frac{\partial \mathbf{U}}{\partial y} + \sigma(x)\mathbf{U} = 0. \tag{4}$$

Type III: Implicit damping with artificial added convection. This method proposed by Freund [12] adds an additional convection term to the governing equations along with the artificial damping. The added convection only takes effect in the buffer zone region. This causes the wave to accelerate towards the outer buffer zone edge. Any reflected waves are slowed by this opposing convection and subjected to more damping than experienced without the additional convection term. The aim being to further reduce the amplitude of any reflected wave before it enters the computational domain. The function for the added convection term is similar to the damping term function

$$U_c(x) = U_{c,\max}\left|1 - \frac{x - L}{L}\right|^{\gamma}, \tag{5}$$

where $U_c(x)$ is the added non-dimensional convective velocity and $U_{c,\max}(x)$ the maximum convective velocity realized at the outer edge of the buffer zone. γ is a shaping parameter similar to β in Eq. (3). The equations solved in the buffer region for Type III buffer boundary now become

$$\frac{\partial \mathbf{U}}{\partial t} + U_c(x)\frac{\partial \mathbf{U}}{\partial x} + [\mathbf{A}]\frac{\partial \mathbf{U}}{\partial x} + [\mathbf{B}]\frac{\partial \mathbf{U}}{\partial y} + \sigma(x)\mathbf{U} = 0. \tag{6}$$

2.2.2. PML boundary condition

The PML boundary condition implemented is the unsplit formulation by Hu [18,19]. For the computational set-up used in the analysis, the boundary condition is implemented in a vertical x-layer only. For which, the PML boundary condition formulation is

$$\frac{\partial \mathbf{U}}{\partial t} + [\mathbf{A}]\frac{\partial \mathbf{U}}{\partial x} + [\mathbf{B}]\frac{\partial \mathbf{U}}{\partial y} + \sigma(x)[\mathbf{B}]\frac{\partial \mathbf{q}}{\partial y} + \sigma(x)\left[\mathbf{U} + \frac{U_0}{1 - U_0^2}[\mathbf{A}]\mathbf{U}\right] = 0, \tag{7}$$

where $\mathbf{q}$ is an auxiliary variable defined as

$$\frac{\partial \mathbf{q}}{\partial t} = \mathbf{U}. \tag{8}$$

2.2.3. Characteristic boundary condition

The performance of the three buffer zone and PML boundary conditions are compared with Thompson's characteristic boundary condition [2,3]. The central concept of Thompson's method is that the Euler equations are hyperbolic in nature and can be decomposed into wave modes of definite velocity, from which specific boundary conditions for the modes can be set. Thompson formulated the boundary condition for the non-linear Euler equations, but the derivation for the LEE is analogous. To construct the characteristic boundary condition

for the x-direction, Eq. (1) is rearranged so that the y-derivative terms are considered as a source term:

$$\frac{\partial \mathbf{U}}{\partial t} + [\mathbf{A}]\frac{\partial \mathbf{U}}{\partial x} = [\mathbf{S}], \quad [\mathbf{S}] = [\mathbf{B}]\frac{\partial \mathbf{U}}{\partial y}. \tag{9}$$

Eq. (9) is then decomposed into its one-dimensional characteristics

$$\begin{aligned} L_1 &= (U_0 - 1)\left(\frac{\partial p'}{\partial x} - \frac{\partial u'}{\partial x}\right), \\ L_2 &= U_0\left(\frac{\partial \rho'}{\partial x} - \frac{\partial p'}{\partial x}\right), \\ L_3 &= U_0\frac{\partial v'}{\partial x}, \\ L_4 &= (U_0 + 1)\left(\frac{\partial p'}{\partial x} - \frac{\partial u'}{\partial x}\right). \end{aligned} \tag{10}$$

The characteristics given in Eq. (10) represent, respectively, the left-travelling acoustic wave, the entropy wave, the vorticity wave and the right-travelling acoustic waves supported by the LEE. The direction of travel of the characteristic determines if it is propagating into or out of the domain. The characteristics that are propagating out of the domain are computed from the solution within the domain and are left unchanged. For a non-reflecting boundary condition, the characteristics of the waves propagating into the domain are set to zero. The equations to be solved at the x-direction boundary are

$$\frac{\partial \mathbf{U}}{\partial t} + \underline{\mathbf{d}} + [\mathbf{B}]\frac{\partial \mathbf{U}}{\partial y} = 0. \tag{11}$$

The vector $\underline{\mathbf{d}}$ is defined as (see Ref. [3])

$$\underline{\mathbf{d}} = \begin{bmatrix} \frac{1}{2}[L_2 + \frac{1}{2}(L_5 + L_1)] \\ \frac{1}{2}(L_5 - L_1) \\ L_3 \\ \frac{1}{2c}(L_5 + L_1) \end{bmatrix}. \tag{12}$$

3. Boundary condition analysis

3.1. Computational set-up

The boundary condition analysis is conducted on the three block Cartesian grid, shown in Fig. 2. Block 1 is the inflow boundary where a downstream travelling two-dimensional plane wave is admitted. A type I buffer zone is used as the inflow condition where $\mathbf{U}_{target}$ is set to the value of

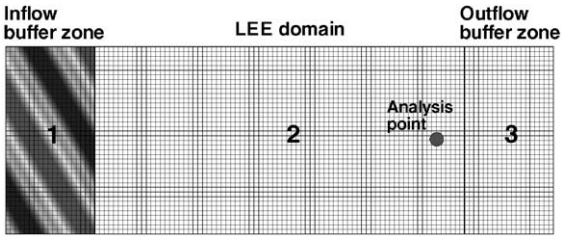

Fig. 2. Computational grid layout for boundary condition analysis.

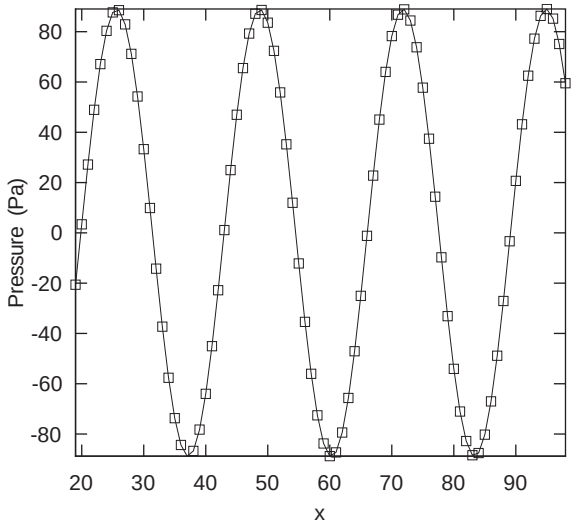

Fig. 3. Cross-section comparison of analytic and numerical solution of a wave propagating through LEE domain. — numerical solution; □ analytic.

the incoming wave. Block 2 is the LEE domain representing the physical domain. Block 3 is the outflow boundary where the non-reflecting boundary conditions are placed. A periodic boundary condition is set for the y-direction boundaries. The size of block 1 is fixed at 20 grid points in the x-direction and 40 in the y-direction. The LEE domain fixed at 80×40 grid points. Block 3 is varied in size during the analysis. For the analysis of Thompson's boundary condition, block 3 is removed and the outflow boundary is set at the downstream edge of block 2 and computed using Eq. (11). The LEE code used for the analysis uses a sixth order prefactored compact spatial discretization scheme [20] and fourth order Runge–Kutta temporal scheme [21]. The code has low dispersion and dissipation characteristics and computes the two-dimensional waves propagated during the analysis with little error, as shown in Fig. 3.

A wavesplitting technique [1] is used to decompose the LEE solution into its vorticity and upstream and downstream propagating acoustic modes. The analysis is conducted at a point just upstream of the outflow boundary condition. At the analysis point the magnitude is computed of the upstream acoustic mode is computed which is assumed to be the reflected wave from the outflow boundary. This allows the magnitude of any reflections to be accurately measured.

3.2. Input wave

The use of transient pressure waves to determine boundary condition performance is a relatively simple test case for which many boundary conditions perform well. The boundary condition performance for more relevant acoustic wave forms is investigated. A two-dimensional plane wave with varying cut-on ratio is used. This allows many features of duct and turbomachinery noise propagation problems to be simulated. At the inflow a sinusoidal pressure wave moving towards the positive y-direction is prescribed: in complex notation

$$p' = 89\mathrm{e}^{\mathrm{i}(\omega t - k_x x - k_y y)}. \tag{13}$$

The peak-to-mean pressure variation of 89 Pa represents a sound pressure level of 130 dB. The ratio of the x-wavenumber (k_x) to y-wavenumber (k_y) can be defined in terms of the cut-on ratio, ξ, as

$$\frac{k_x}{k_y} = \frac{-U_0\xi + \sqrt{\xi^2 - 1}}{\sqrt{1 - U_0^2}}. \tag{14}$$

The corresponding angular frequency, ω, is

$$\omega = \xi k_y \sqrt{1 - U_0^2}. \tag{15}$$

Varying the cut-on ratio allows the wave frequency and wave angle of the input wave to be varied. Here, the wave angle is defined as the angle made between the wavefront normal and the outward normal of the boundary condition edge.

3.3. Two-dimensional wavesplitting

The LEE support entropy, vorticity and acoustic wave modes. Wavesplitting allows the LEE equations to be decomposed into these constitutive modes. Wilson's [1] wavesplitting method applied to two-dimensional plane waves is presented. The analysis begins with the LEE in primitive form, given by Eq. (1). To simplify the analysis, the flow is assumed to be isentropic, i.e., $p/\rho^{\gamma} = constant$. This allows the LEE to be reduced to the following form:

$$\frac{\partial \mathbf{U}^1}{\partial t} + [\mathbf{A}^1]\frac{\partial \mathbf{U}^1}{\partial x} + [\mathbf{B}^1]\frac{\partial \mathbf{U}^1}{\partial y} = 0, \tag{16}$$

$$\mathbf{U}^1 = \begin{bmatrix} u' \\ v' \\ p' \end{bmatrix},$$

$$[\mathbf{A}^1] = \begin{bmatrix} U_0 & 0 & 1 \\ 0 & U_0 & 0 \\ 1 & 0 & U_0 \end{bmatrix}, \quad [\mathbf{B}^1] = \begin{bmatrix} 0 & 0 & 0 \\ 0 & 0 & 1 \\ 0 & 1 & 0 \end{bmatrix}.$$

Next, the $\partial/\partial x$ terms are collected on the left hand side and the Fourier transform of the remaining terms on the right hand side in time and y-direction performed. This gives

$$\begin{bmatrix} U_0 & 0 & 1 \\ 0 & U_0 & 0 \\ 1 & 0 & U_0 \end{bmatrix} \frac{\partial \mathbf{U}^1}{\partial x} = \begin{bmatrix} -\mathrm{i}\omega & 0 & 0 \\ 0 & -\mathrm{i}\omega & \mathrm{i}k_y \\ 0 & \mathrm{i}k_y & -\mathrm{i}\omega \end{bmatrix} \mathbf{U}^1. \tag{17}$$

This equation is in the form

$$[\mathbf{A}^1] = \frac{\partial \mathbf{U}^1}{\partial x} = [\mathbf{B}^1]\mathbf{U}^1 \tag{18}$$

or

$$\frac{\partial \mathbf{U}^1}{\partial x} = [\mathbf{A}^1]^{-1}[\mathbf{B}^1]\mathbf{U}^1. \tag{19}$$

The eigenvalues of $[\mathbf{A}^1]^{-1}[\mathbf{B}^1]$ are, in order of magnitude

$$\begin{aligned} \lambda_1 &= \frac{-U_0\omega - \sqrt{\omega^2 - k_y^2(1-U_0^2)}}{(1-U_0^2)}, \\ \lambda_2 &= \frac{\omega}{U_0}, \\ \lambda_3 &= \frac{-U_0\omega + \sqrt{\omega^2 - k_y^2(1-U_0^2)}}{(1-U_0^2)}, \end{aligned} \tag{20}$$

λ_1 and λ_3 represent the downstream and upstream travelling acoustic waves, respectively. λ_2 represents the vorticity. The inverse of the corresponding eigenvector matrix gives the coefficients for the LEE modes.

$$[\mathbf{E}^{-1}] = (\mathbf{e}_1\,\mathbf{e}_2\,\mathbf{e}_3)^{-1} = \begin{bmatrix} \dfrac{\omega}{(1-U_0^2)(\lambda_x-\lambda_x)} & \dfrac{U_0^2K_y}{(1-U_0^2)(\lambda_x-\lambda_x)} & \dfrac{1}{2} \\ \dfrac{k_y^2U_0^2}{\omega^2+k_y^2U_0^2} & -\dfrac{\omega k_y U_0}{\omega^2+k_y^2U_0^2} & \dfrac{k_y^2U_0^2}{\omega^2+k_y^2U_0^2} \\ -\dfrac{\omega}{(1-U_0^2)(\lambda_x-\lambda_x)} & -\dfrac{U_0^2K_y}{(1-U_0^2)(\lambda_x-\lambda_x)} & \dfrac{1}{2} \end{bmatrix}. \tag{21}$$

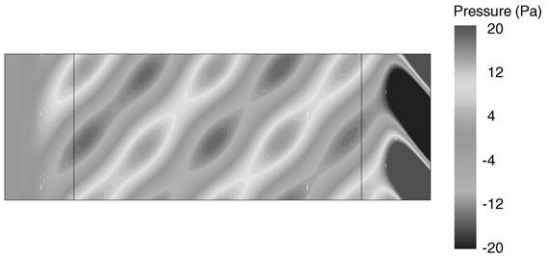

Fig. 4. Error contour plot showing magnitude of acoustic wave reflected from outflow boundary for cut-on ratio, $\xi = 1.5$.

In terms of the definitions in Eqs. (14) and (15), the coefficient matrix is

$$[\mathbf{E}]^{-1} = \begin{bmatrix} \dfrac{\xi}{2\sqrt{\xi^2-1}} & \dfrac{U_0}{2\sqrt{\xi^2-1}\sqrt{1-U_0^2}} & \dfrac{1}{2} \\ -\dfrac{\xi U_0\sqrt{1-U_0^2}}{\xi^2(1-U_0^2)+U_0^2} & -\dfrac{\xi^2(1-U_0^2)}{\xi^2(1-U_0^2)+U_0^2} & -\dfrac{\xi\sqrt{1-U_0^2}}{\xi^2(1-U_0^2)+U_0^2} \\ -\dfrac{\xi}{2\sqrt{\xi^2-1}} & -\dfrac{U_0}{2\sqrt{\xi^2-1}\sqrt{1-U_0^2}} & \dfrac{1}{2} \end{bmatrix}. \tag{22}$$

The non-dimensional value for the upstream and downstream travelling acoustic wave and the vorticity wave in Fourier space is then given by

$$[p^{us}_{\omega,k_y} \;\; V^{vort}_{\omega,k_y} \;\; p^{ds}_{\omega,k_y}]^{\mathrm{T}} = [\mathbf{E}]^{-1}[u_{\omega,k_y} \;\; v_{\omega,k_y} \;\; p_{\omega,k_y}]^{\mathrm{T}}. \tag{23}$$

Hence

$$p^{us/ds}_{\omega,k_y} = \frac{1}{2}\left(p_{\omega,k_y} \pm \frac{\xi}{\sqrt{\xi^2-1}} u_{\omega,k_y} \pm \frac{U_0}{\sqrt{\xi^2-1}\sqrt{1-U_0^2}} v_{\omega,k_y} \right). \tag{24}$$

From Eq. (24) the magnitude of the reflected (upstream) pressure wave can be computed. A typical example of the form of the upstream (reflected) wave is shown in Fig. 4 which is a contour plot showing the error in the computed and analytic solution produced by type II buffer zone for a wave with a cut-on ratio of 1.5. The large error in the outflow buffer zone confirms that solutions in such zones are not physical. The reflected wave is damped at the inflow boundary due to the use of a buffer zone as an inflow boundary condition also.

4. Results and discussion

The performance of non-reflecting boundary conditions can depend on a number of different factors: the cut-on ratio, frequency/wavelength and wave angle of the out-going wave, mean flow

velocity and in the case of buffer zone boundary conditions, the damping rate and buffer zone length. We investigate the effect of these parameters on the performance of the PML and the three different types of buffer zone implementations mentioned in Section 2.2.1. To investigate the effect of the wave cut-on ratio and wave angle on buffer zone performance, the cut-on ratio of the input wave was varied and the reflected wave for a fixed buffer length of 20 grid points measured. The values of σ_{max} and β were fixed at 1.0 and 3.0, respectively. For type III buffer, the values of

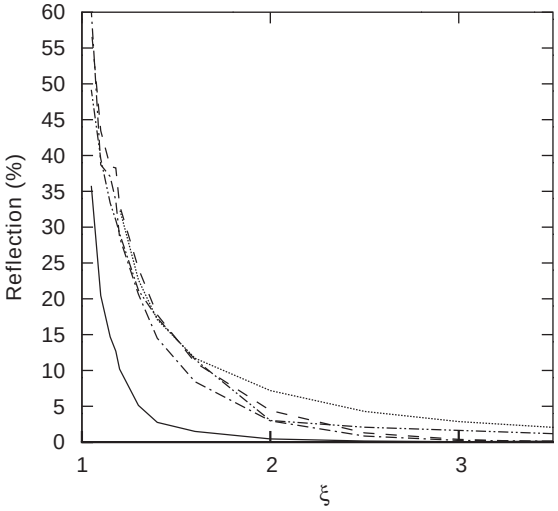

Fig. 5. Reflection with varying cut-on ratio, ξ. Fixed 20 grid point buffer zone length. — type I, – – – type II, - · - type III, ... Thompson and - ·· - PML.

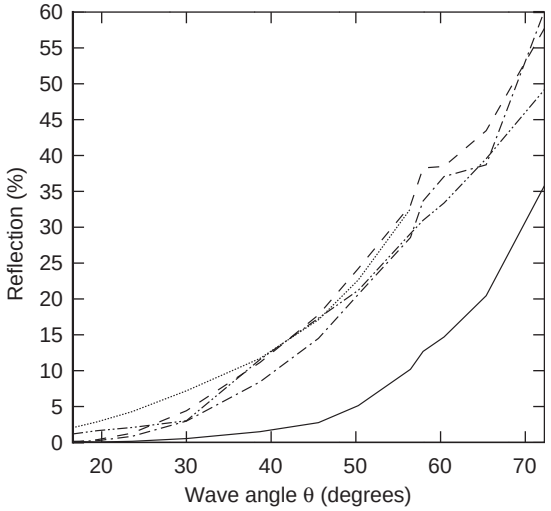

Fig. 6. Reflection with varying wave angle, θ. Fixed 20 grid point buffer zone length. — type I, – – – type II, - · - · - type III, ... Thompson and - ·· - ·· - PML.

$U_{c,\max}$ and γ were fixed at 1.15 and 2, respectively. The difference in the values for β and γ causes a greater proportion of the artificial convection to occur ahead of the damping, increasing the time spent by any reflected waves in the damping region. Fig. 5 shows the percentage of the 89 Pa incident wave reflected by the three different buffer implementations and Thompson's boundary condition for varying values of cut-on ratio, ξ, with no background mean flow. The change in cut-on ratio varies the wave angle with respect to the boundary normal according to Eq. (14). The corresponding results for wave angle are shown in Fig. 6. As can be seen, for all five boundary conditions a reduction in the cut-on ratio, or correspondingly, an increase in the incident wave angle causes an exponential increase in the magnitude of the reflected wave. Type I buffer zone performs the best, but still produces large reflections at high wave angles. The Thompson boundary condition performs similarly to the PML, types II and III buffer zones at this buffer length. The improved performance for type I buffer zone may be explained in part by the effect of the different damping types on the wave within the buffer zones. Fig. 7 shows the effect of damping of the different buffer zone type on the wave within the outflow buffer zone. The

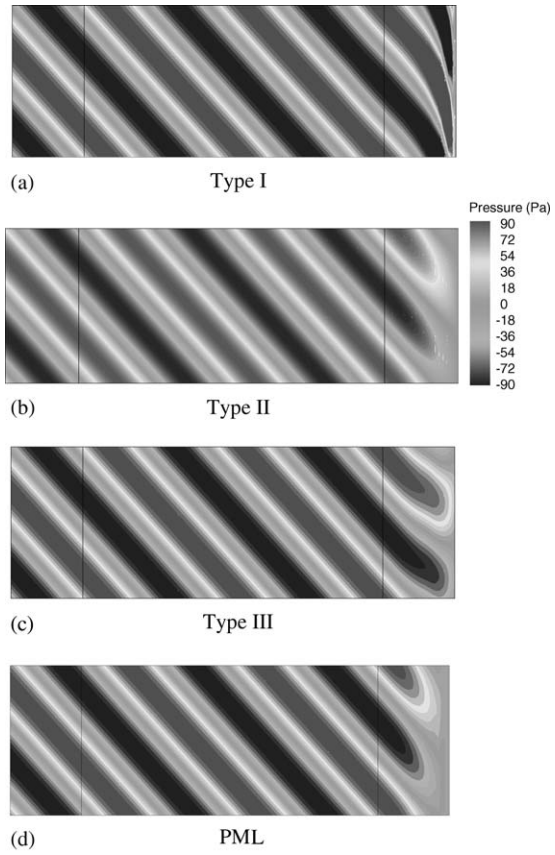

Fig. 7. Contour plots showing the effect of the different damping methods on the wave in the outflow buffer zone. Contour levels are the same for each plot.

damping for type I buffer zone is applied to the solution vector and not the rate of change of the solution vector. This forces the waves to fold up, causing the wave angle to reduce. Type II boundary applies damping to the rate of change of the solution vector and the wave angle remains unaltered. The artificial convection included in the Type III implementation causes the wave angle to increase. This effective increase in the wave angle may offset any potential reduction in reflection caused by the artificial convection as intended. Fig. 7 also shows that the effect of damping of type II buffer zone and the PML is very similar. Examining Eqs. (4) and (7) shows that for this test case set-up, the PML condition is different to type II buffer zone condition only in the introduction of the auxiliary variable **q** and the mean flow modification of the damping on the solution vector **U**. The similarity of the damping shown in Fig. 7 suggests that the damping term involving the solution vector is dominant, with the auxiliary variable damping term having only a small effect. This results in the similar performance of the PML and type II buffer, shown in Figs. 5 and 6.

With the introduction of a background mean flow, the performance of the three buffer zone implementations and the PML are analyzed under more realistic conditions. Two test cases are conducted with the introduction a background mean flow of $U_0 = 0.4$, $U_0 = -0.4$, simulating an outflow and inflow boundary, respectively. The buffer zone length is again fixed at 20 grid points and the same parameters for the damping and artificial convection maintained from the previous fixed buffer test case. Results for the $U_0 = 0.4$ case are shown in Fig. 8. The effect of this positive mean flow is to increase the wave angle and decrease the wave frequency for a set cut-on ratio. The figures show a similar trend to the no mean flow case, with a reduction in performance with reduced cut-on ratio and higher incident wave angle. Results for the $U_0 = -0.4$ case, simulating an inflow condition, are shown in Fig. 9. Again, type I buffer zone, using explicit damping gives the best performance over the range of cut-on ratios simulated.

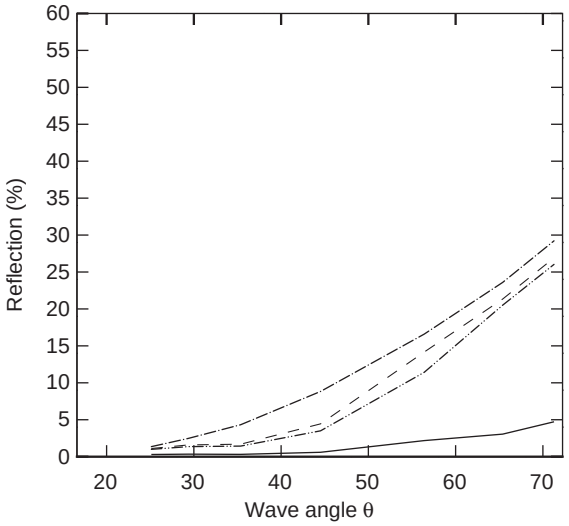

Fig. 8. Reflection with varying wave angle, θ. Fixed 20 grid point buffer zone length. Mean flow, $U_0 = 0.4$. — type I, – – – type II, - · - · - type III and - ·· - ·· - PML.

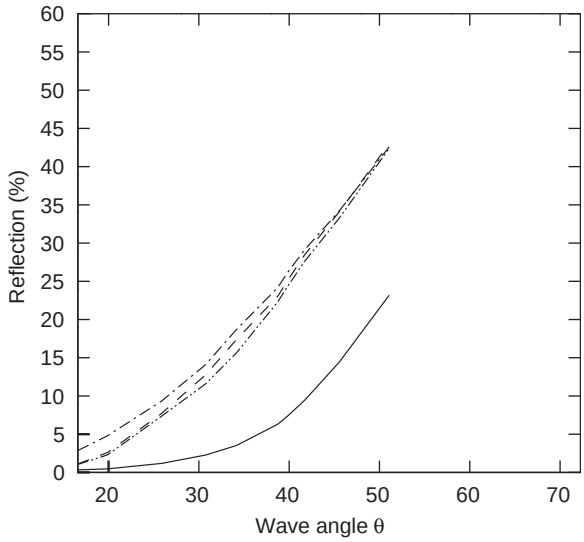

Fig. 9. Reflection with varying wave angle, θ. Fixed 20 grid point buffer zone length. Mean flow, $U_0 = -0.4$. — type I, – – – type II, - · - · - type III and - ·· - ·· - PML.

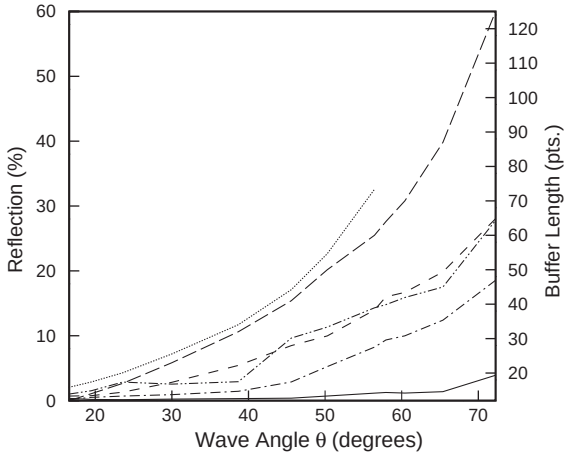

Fig. 10. Reflection with varying wave angle, θ. The buffer zone length is set equal to the x-direction wavelength of the out-going wave. — type I, - - - type II, - · - · - type III, ... Thompson, - ·· - ·· - PML and – – – Buffer length.

To investigate the effect of buffer length on buffer zone performance, we vary the outflow buffer zone length to match the change in wavelength in the x-direction as the cut-on ratio is varied. The parameters for the damping and artificial convection are kept the same as those used in the previous fixed buffer length analysis. The results of the no mean flow case are shown in Fig. 10 and comparison with Fig. 6 clearly shows that tuning the buffer length gives a marked improvement in performance, particularly for type I buffer zone. For a wave angle of 72° only a 4

percent reflection was observed. The corresponding buffer zone length used for the different wave angles is also shown. In order to reduce the reflection for type I buffer zone with a 72° incident wave to 4 percent however, the buffer length had to be extended to 125 grid points; longer than the LEE domain itself. Reducing the cut-on ratio also causes the x-wavenumber, k_x, to increase. Hence, the results shown in Fig. 10 represent the effect of wave angle and x-wavelength of the out-going wave on the buffer zone performance. We can separate these effects by analyzing the performance for a fixed wave angle but varying x-wavelength. This is simply achieved by varying the length of the domain in the y-direction. To maintain the periodic boundary condition the value for the y-wavelength must change also. Keeping the cut-on ratio constant causes the x-wavelength to change according to Eq. (14). Fig. 11 shows the variation in the performance of type I buffer zone with x-wavelength for a fixed wave angle of 45° and fixed buffer length of 20 grid points. The figure shows that an increasing x-wavelength of the out-going wave also causes an increase in reflection. Hence, both the wave angle and wavelength component in the direction of damping are important out-going wave characteristics affecting buffer zone performance.

The effect of the mean flow velocity and damping rate may be analyzed together. Too little damping causes the out-going wave to reach the outer buffer zone edge causing large reflections or even unstable solutions in some cases. Too much damping causes the effect of the damping to become so advanced that the out-going wave is fully damped near the interface between the computational domain and the buffer zone and the majority of the buffer zone length is not utilized. For the damping function given by Eq. (3), the effect of varying the value of β is shown in Fig. 12. The amount of damping is related to the area under the damping curve, the greater the value of β, the less damping applied. Fig. 13 shows the performance of type I buffer zone with varying mean flow velocity (non-dimensionalized by the speed of sound) and damping rate. The buffer zone is fixed at 20 grid points and the cut-on ratio fixed at 2. Eq. (14) shows that for a fixed value of ξ, an increase in the Mach number increases the wave angle which is a main cause of increased reflected wave amplitude. This accounts for the increase in reflection with U_0 at fixed

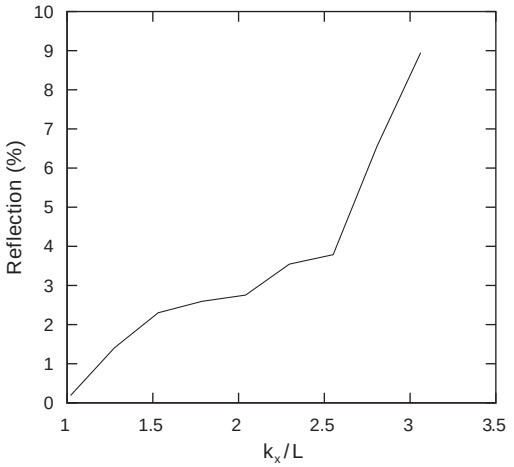

Fig. 11. The effect of x-wavelength on performance. x-wavelength is given as a ratio of buffer length, L. — Wave angle = 45°.

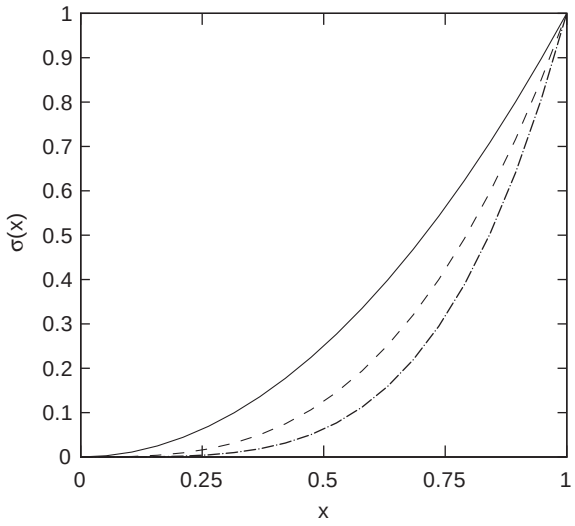

Fig. 12. Damping function for different values of β. — $\beta = 2$, – – – $\beta = 3$, - · - · - $\beta = 4$.

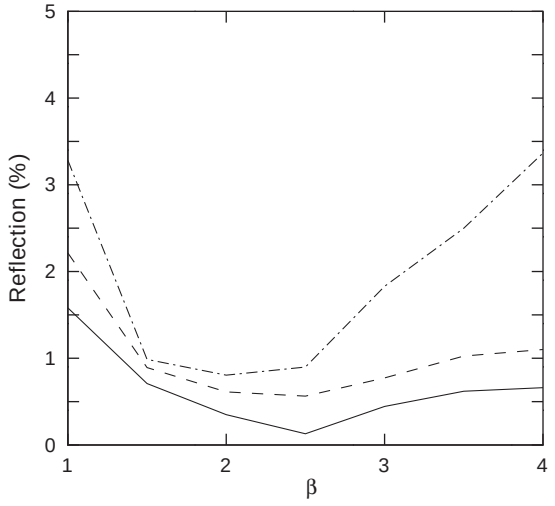

Fig. 13. Effect of damping rate on type I buffer zone performance. Cut-on ratio, $\xi = 2$; fixed 20 grid point buffer length. — $U_0 = 0.0$, – – – $U_0 = 0.4$ and - · - · - $U_0 = 0.8$.

values of β. Fig. 13 shows that for a given value of U_0 there is an optimum value for β. An increased mean flow means that the speed at which waves enter the buffer zone is greater, this requires a greater amount of damping, signified by a reduced value of β. However, up to Mach numbers of 0.8, the change in β required is relatively small and values of between 2 and 2.5 will ensure a damping rate near the optimum over the range of Mach numbers.

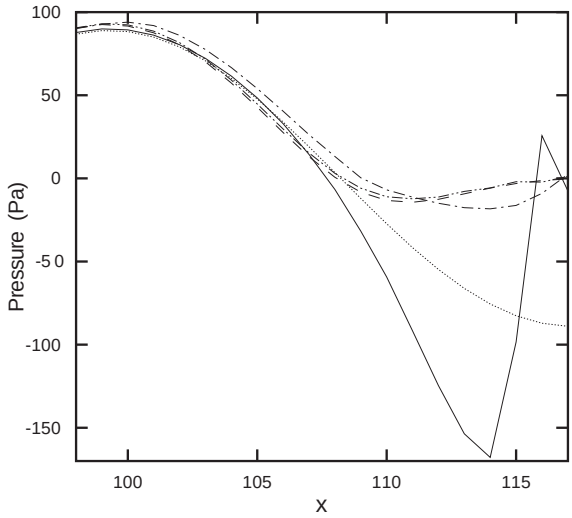

Fig. 14. Comparison of typical damped solutions for the buffer zone types in the outflow buffer zone, $\xi = 1.5$; fixed 20 grid point buffer length. — type I, – – – type II, - · - · - type III, - ·· - ·· - PML and ..... analytic solution.

The results of the buffer zone analysis showed that type I buffer zone, which explicitly damped the solution vector after each timestep, performed the best. This is remarkable as the explicit damping causes the waves to fold up within the buffer zone, giving an erratic solution within the buffer zone compared to the smooth damping created by types II and III buffer zone and PML (see Fig. 14). The results also showed that types II and III buffer zones gave similar performance for the fixed buffer length test cases. But for larger buffer zone lengths, type III buffer zone gave noticeably improved results compared to type II buffer zone. The only difference between these two implementations is the artificial convection added in type III buffer zone. Hence, the inclusion of the artificial convection can have a positive effect in reducing the reflected wave and more investigation into the effect of the convective term than studied in this paper may give further improvements in performance. However, the artificial convection is most effective when the majority of the convection takes place before the damping and not simultaneously. This requires the separation of the buffer zone into a convective and damping region, which in order to generate the required amount of damping, requires larger buffer zones. Hence, even though further improvement may be possible it is expected that, for a given buffer length, the performance of type I buffer zone implementation cannot be matched.

The main factors affecting the buffer zone performance are the damping rate and the wavelength, wave angle and frequency of the out-going wave. The damping rate depends upon the shape of the damping function and the mean flow velocity in the direction of the damping—the greater the mean flow velocity the greater the amount of damping required. For the different mean flows tested, different optimum values of damping rate (controlled by the parameter β) were found. However, up to a mean flow of Mach number 0.8, the variation in the value of β for the optimum value was small and a value of between 2 and 2.5 for β has been confirmed as being most suitable for subsonic mean flows. Wave angle has the greatest affect on buffer zone performance. For angles up to 30°, type I buffer zone with a fixed buffer length of 20 grid points gives adequate

results. Greater wave angles give rise to large reflections. The most effective way to reduce such reflections is to increase the buffer zone length. However, as has been shown, for out-going waves nearly parallel to the outflow boundary, very large buffer zones are required which become computationally expensive. The effect of the out-going wavelength is to change the required buffer length. For fixed wave angles, larger wavelengths require buffer zones of increased length. The influence of wave angle and wavelength on buffer zone performance means that a general method for defining minimum length buffer zones for adequate performance is difficult as buffer zone performance is problem specific.

5. Conclusions

The performance of five non-reflecting boundary conditions for the linearized Euler equations has been investigated using a two-dimensional wavesplitting technique. Wavesplitting allows the decomposition of the linearized Euler equations into upstream and downstream acoustic eigenmodes modes, allowing reflected waves from domain boundaries to be accurately measured. The technique was applied to the performance of three different implementations of the buffer zone boundary condition. The results showed that a buffer zone boundary condition which uses explicit damping performs best. For all boundary conditions, a deterioration in performance was observed for higher out-going wave angles. Extension of the buffer zone length significantly reduced wave reflections. However, for the explicit damping buffer zone, buffer lengths of the order of one wavelength of the incident wave in the direction of damping were required to produce satisfactory results. This requirement could greatly increase computational cost. For each different incident waveform tested, there was an optimum value for the amount of damping to be applied. For higher mean flow speeds, a greater amount of damping was required to obtain the optimum performance.

References

[1] A.G. Wilson, A method for deriving tone noise information from CFD calculations on the aeroengine fan stage, *NATO RTO-AVT Symposium on Developments in Computational Aero- and Hydro-Acoustics*, Manchester, UK, 8–11 October 2001.

[2] K.W. Thompson, Time-dependent boundary conditions for hyperbolic systems, I, *Journal of Computational Physics* 68 (1987) 1–24.

[3] K.W. Thompson, Time-dependent boundary conditions for hyperbolic systems, II, *Journal of Computational Physics* 89 (1990) 439–461.

[4] T.J. Poinsot, S.K. Lele, Boundary conditions for direct simulations of compressible viscous flows, *Journal of Computational Physics* 101 (1992) 104–129.

[5] M.B. Giles, Non-reflecting boundary conditions for Euler equation calculations, *American Institute of Aeronautics and Astronautics Journal* 28 (1990) 2050–2058.

[6] R. Hixon, S.-H. Shih, R.R. Mankbadi, Evaluation of boundary conditions for the gust-cascade problem, *Journal of Propulsion and Power* 16 (2000) 72–78.

[7] R.R. Mankbadi, R. Hixon, S.-H. Shih, L.A. Povinelli, Use of linearized Euler equations for supersonic jet noise prediction, *American Institute of Aeronautics and Astronautics Journal* 36 (1998) 140–147.

[8] A. Bayliss, E. Turkel, Radiation boundary conditions for wave-like equations, *Communications on Pure and Applied Mathematics* 33 (1980) 708–725.

[9] C.K. Tam, J.C. Webb, Dispersion-relation-preserving finite difference schemes for computational acoustics, *Journal of Computational Physics* 107 (1993) 262–281.
[10] B. Wasistho, B.J. Guerts, J.G.M. Kuerten, Simulation techniques for spatially evolving instabilities in compressible flow over a flat plate, *Computers and Fluids* 7 (1997) 713–739.
[11] S.S. Collis, S.K. Lele, A computational approach to swept leading-edge receptivity, American Institute of Aeronautics and Astronautics Paper 1996-0180.
[12] J.B. Freund, Proposed inflow/outflow boundary conditions for direct computation of aerodynamic sound, *American Institute of Aeronautics and Astronautics Journal* 35 (1997) 740–742.
[13] T. Colonius, S.K. Lele, P. Moin, Boundary conditions for direct computation of aerodynamic sound, *American Institute of Aeronautics and Astronautics Journal* 31 (1993) 1574–1582.
[14] S. Ta'asan, D.M. Nark, An absorbing buffer zone technique for acoustic wave propagation, American Institute of Aeronautics and Astronautics Paper 95-0164.
[15] J.P. Berenger, A perfectly matched layer for the absorption of electromagnetic waves, *Journal of Computational Physics* 114 (1994) 185–200.
[16] F.Q. Hu, On absorbing boundary conditions of linearized Euler equations by a perfectly matched layer, *Journal of Computational Physics* 129 (1996) 201–219.
[17] S. Arbabanel, D. Gottlieb, J.S. Hesthaven, Well-posed perfectly matched layers for advective acoustics, *Journal of Computational Physics* 154 (1996) 266–283.
[18] F.Q. Hu, A stable, perfectly matched layer for linearized Euler equations in unsplit physical variables, *Journal of Computational Physics* 173 (2001) 455–480.
[19] F.Q. Hu, On constructing stable perfectly matched layers as an absorbing boundary condition for Euler equations, American Institute of Aeronautics and Astronautics Paper 2002-0227.
[20] R. Hixon, Prefactored small-stencil compact schemes, *Journal of Computational Physics* 165 (2000) 522–541.
[21] F.Q. Hu, M.Y. Hussaini, J.L. Manthey, Low-dissipation and low dispersion Runge–Kutta schemes for computational acoustics, *Journal of Computational Physics* 124 (1996) 177–191.